Application of Adaptive Image Processing Technique to Real-Time Spatial Compound Ultrasound Imaging Improves Image Quality

Jean-Yves Meuwly, MD, Jean-Philippe Thiran, PhD,† and François Gudinchet, MD**

Rationale and Objectives. To assess the impact of adaptive filter postprocessing on quality of ultrasound images.
Methods. Ultrasound images acquired with real-time spatial compound imaging (SonoCT imaging) were subsequently processed with an adaptive real time algorithm (XRES imaging). Conventional and XRES-processed images from abdominal, pediatric or small parts ultrasound explorations were compared. The delineation of borders, tissue contrast, amount of noise, and overall image quality were evaluated.
Results. Delineation of borders and tissue contrast were improved on all images ($P < 0.05$). The amount of noise was reduced ($P < 0.05$). The overall image quality was improved for abdominal, pediatric and small parts ultrasound explorations ($P < 0.05$). No image degradation was found.
Conclusions. Adaptive processing provided better image quality without loss of clinically useful information.

Key Words: diagnostic imaging, medical electronics, image enhancement, ultrasonography

(*Invest Radiol* 2003;38: 257–262)

Many innovative technologies, such as harmonic imaging[1–4] and real-time compound imaging (SonoCT imaging),[5–8] have been introduced over the past several years to improve ultrasound (US) image quality. Real-time processing involving adaptive image analysis and enhancement (XRES imaging) is one of the latest commercially available US techniques. It derives from processing of digital signals and is based on research originally performed for use in enhancing MRI images. With this technology, the US image, initially constructed by the scan converter of the device, is further refined in real time by an adaptive algorithm prior to display on the screen.

XRES imaging is considered adaptive because it adapts its processing automatically to the nature of the target, both locally (ie, within an individual image) and temporally (over time from image to image). This adaptability is achieved in XRES by having both an analysis phase, in which both real tissue structures and ultrasound artifacts are identified, and an enhancement phase, in which structures identified in the analysis phase are enhanced and artifacts are suppressed. The analysis phase of XRES takes into account many characteristics of the image, such as textural and structural properties including gradients and local statistics. The results of this analysis directly control the enhancement phase; for example, smoothing is applied along an interface to improve continuity, whereas edge enhancement is applied in the perpendicular direction to improve spatial resolution. In regions identified by the analysis phase as being relatively homogeneous (containing minimal structure or texture), smoothing is applied equally in all directions to suppress speckle and noise. Thus XRES is designed both to suppress artifacts and to enhance interfaces and margins. In addition, XRES is a multiresolution algorithm. This means that all processing—analysis and enhancement—occurs at multiple scales within the image. Multiresolution processing improves robustness by allowing the XRES algorithm to adapt itself to variations in artifacts and feature scale as well as to the variable size of anatomic structures. It is somewhat similar to a human observer looking at an image from different distances to perceive relevant features at different scales.

The XRES processing has the potential to enhance boundaries, structures and edges and to reduce noise, speckle and clutter, and finally, to improve overall clinical US image quality.

The purpose of our study was to prospectively compare real-time compound imaging (SonoCT imaging) and the addition of the XRES algorithm for US images of abdominal,

Received for publication August 12, 2002; accepted January 22, 2003.
From the *Department of Diagnostic and Interventional Radiology, University Hospital, Lausanne, Switzerland; and the †Signal Processing Institute, Swiss Federal Institute of Technology, Lausanne, Switzerland.
Reprints: Jean-Yves Meuwly, MD, Department of Diagnostic and Interventional Radiology, University Hospital, Rue du Bugnon 46, Lausanne, Switzerland. Jean-Yves.Meuwly@chuv.hospvd.ch

0020-9996/03/3805-0257
DOI: 10.1097/01.RLI.0000064337.62114.32

small-parts and pediatric applications and to determine whether this processing improves image quality.

MATERIALS AND METHODS

Patient Population

From August to September 2001, 30 patients (15 men, 15 women, mean age 38) were studied by using real time compound imaging with and without XRES processing. Ten patients (4 men, 6 women; age range, 44-84 years; mean age, 63 years) were referred for abdominal US examination. Ten (5 men, 5 women; age range, 27-79 years; mean age, 50) for small parts US examination, and 10 (6 men, 4 women; age range, 1 week-10 years; mean age, 4 years) were referred for pediatric US examination. The most frequent indications for abdominal explorations were abdominal pain or screening for metastasis. For small parts examinations, indications included breast lump, soft parts swelling or testicular mass. Pediatric cases consisted of examinations for abdominal pain or screening for hip, renal or brain abnormality.

Imaging

All studies were performed with an ATL HDI® 5000 ultrasound system (Philips Ultrasound, Bothell, WA). A 5-2 MHz curved array transducer was used for abdominal examinations. A 12-5 MHz linear array transducer was used for small parts. A 7-4 MHz curved array or a 12-5 MHz linear array transducer was used for pediatric explorations. Clinically useful images were acquired by sonographers, according to ACR/AIUM standard imaging protocols, using real-time compound imaging (SonoCT imaging), without adaptive processing. Adaptive processing was subsequently applied to these freeze-frames, as described below. Both images (with and without XRES adaptive processing) were stored on the hard disk of the US machine and then sent to the central archive system in DICOM format. XRES images were not used for diagnostic purpose at this time of the study.

Description of the Xres Image Processing Algorithm

As depicted in the block diagram of Figure 1, the main steps in the image processing chain were the following:

A: Laplacian Pyramid Decomposition

The scan-converted image frame was processed within a Laplacian pyramid according to the standard procedure defined by Burt and Adelson in 1983.[9] Each image frame was decomposed into a succession of sub-bands each representing a level of resolution going from fine to coarse. Processing of the sub-bands was then performed within an analysis and a filtering phase as described below.

B: Analysis Phase Within Each of the Pyramid Sub-Bands

Each of the sub-bands was segmented into:

- Low-contrast textured regions dominated by noise and speckle,
- Higher contrast regions containing specular reflectors.

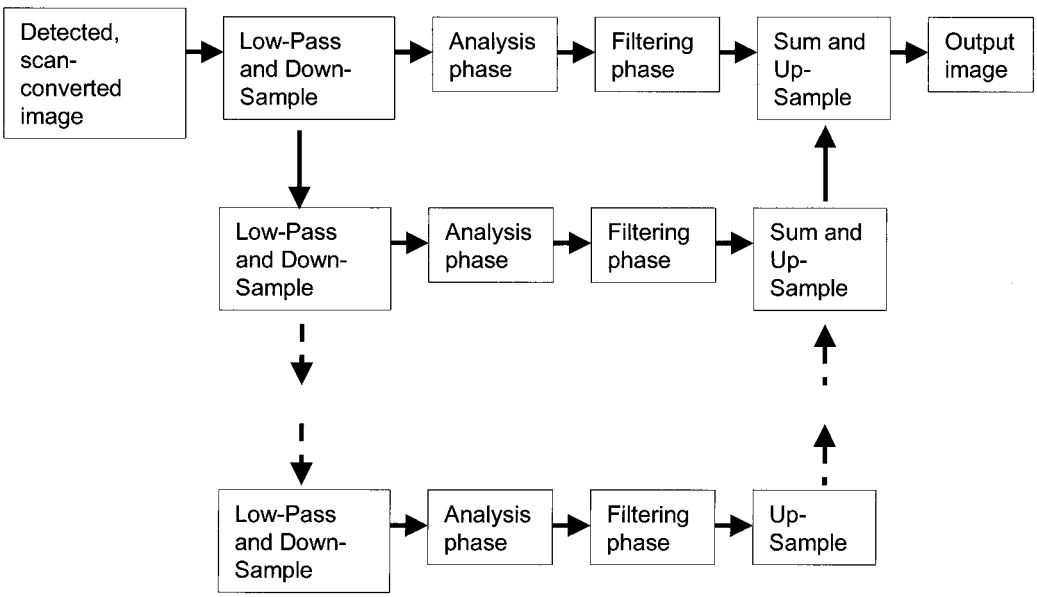

FIGURE 1. Schematic representation of the main processing steps of the XRES algorithm. The scan-converted image frame is decomposed into a succession of sub-bands, which are subsequently processed within an analysis and a filtering phase. The processed sub-bands are finally combined to produce the output image.

Within the high-contrast region, the degree of local anisotropy was determined by using the structure tensor as defined by Weickert.[10] Such a tensor is a mathematical entity providing a convenient assessment, for each pixel, of whether the local image feature is anisotropic, as can be expected for specular reflectors; if it is the case, this tensor also allows determining in which spatial direction the signal is the strongest. Mathematically speaking, the anisotropy assessment was deduced from the eigenvector analysis of the image gradient-based structure tensor. In the current 2-dimensional (2D) case, there were 2 orthogonal eigenvectors, each associated with an eigenvalue describing the signal energy in its direction. A feature was classified as anisotropic if the ratio of large to small eigenvalue was above 2; otherwise, the feature was classified as isotropic.

C: Filtering Phase Within Each of the Pyramid Sub-Bands

From the above described segmentation and feature-anisotropy analysis, the image processing step within each of the pyramid sub-bands was performed in such a way that:

- In the low contrasted textured regions or for isotropic-class features in the high-contrast region, a slight isotropic smoothing was performed,
- For other situations (ie, anisotropic features in the high-contrast region), smoothing was performed by using an anisotropic kernel with a long support along the low-contrast structure-tensor direction and a short support along the high-contrast structure-tensor direction.

D: Combining the Processed Pyramid Sub-Bands to Produce the Output Image

After performing the above procedure, the processed sub-bands were up-sampled and combined together by using the usual Burt and Adelson procedure.[9]

All above analysis and processing steps were executed in real time (more than 15 frames per second).

Image Analysis

Electronically stored images were retrieved from the archive and saved in JPEG (using a compression rate of 10:1) format on a local computer (Compaq, PIII, 600 MHz, 256 Mb RAM), using the MagicView software (Siemens, Erlangen, Germany). All demographic and technical information was removed from images. Then the images were arranged by pair. The layout of the paired images was random. These pairs were subsequently randomly displayed on a large plasma screen (Flat Panel Monitor PFM-42B1, Sony Corporation, Japan). The paired images (Fig. 2) were compared side by side by 2 radiologists experienced in US (JYM, FG). The 2 readers, who were blinded with regard to the clinical diagnosis, consensually evaluated the sets of images for the following criteria: (*i*) delineation of borders, (*ii*) tissue contrast, (*iii*) amount of noise, and (*iv*) overall image quality. A set of 360 images was evaluated.

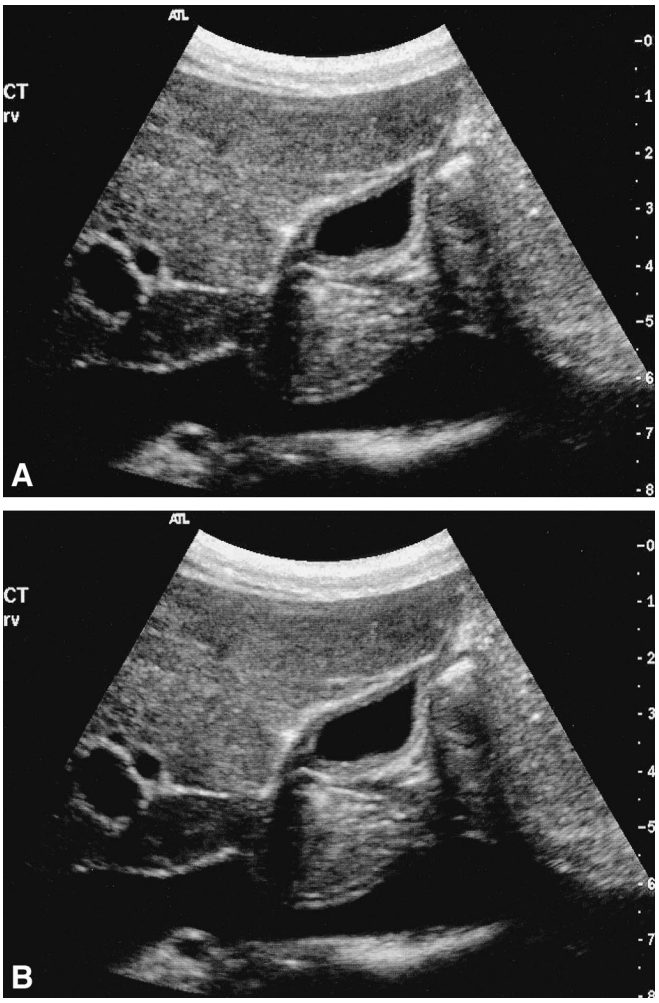

FIGURE 2. Longitudinal view of the right upper abdomen. Liver, gallbladder, right portal vein and inferior vena cava are visible. A, Compound image. B, XRES image. No technical or demographic data are visible

A 6-point rating scale was used, with 1 as the lowest grade and 6 as the highest. For delineation of anatomic structure borders, a score of 1 depicted very low delineation; 2, low delineation; 3, moderate delineation; 4, high delineation; 5, very high delineation; and 6, optimal delineation. For tissue contrast, 1 indicated very low; 2, low; 3, moderate; 4, high; 5, very high; and 6, optimal tissue contrast. Concerning the amount of noise, 1 indicated blurred and not interpretable image; 2, blurred but interpretable image; 3, much noise; 4, little noise; 5, very little noise; and 6 no visible noise. For overall image quality, 1 indicated very low; 2, low; 3, moderate; 4, high; 5, very high and 6, optimal image quality.

As US is basically a dynamic imaging technique and comparisons were made with freeze frames, no evaluation of diagnostic efficiency or abnormality conspicuity was performed. For each image, the presence or absence of abnormalities of the different tissues and organs, as well as the differences in a pair were reported.

Statistical Analyses

Nonparametric statistical methods were used. To compare modality performances based on the ordinal scaled criteria, we used the Wilcoxon pairwise signed-rank tests. To compare median scores for each modality and technique, we used the Kruskal–Wallis one-way analysis of variance by ranks. Two-tailed P values were used, and values less than 0.05 were considered as statistically significant. The computations were performed by using the STATA package (Version 7, Stata Corporation, College Station, TX).

RESULTS

Abdominal Imaging

The median scores of the compound and XRES abdominal examinations for all criteria are shown in Table 1. Regarding abnormality detection, compound and XRES imaging depicted the same 53 normal findings and 27 abnormalities. Abnormalities included biliary cysts in 9 images, fatty liver in 7 images, cholecystolithiasis in 5 images, cholecystitis in 2 images, pancreatic pseudocyst in 2 images, liver metastasis in one image, and renal cyst in one image.

Small Parts Imaging

The median scores of the compound and XRES small parts examinations for all criteria are shown in Table 2. Regarding abnormality detection, compound imaging depicted 18 normal findings and 32 abnormalities. Abnormalities included breast cysts in twelve images, subcutaneous lymphangioma in 4 images, hydrocele in 4 images, fibroadenoma in 3 images, testicular calcification in 2 images, subcutaneous edema in 2 images, breast scar in one image, breast cancer in one image, subcutaneous metastasis in one image, liponecrosis in one image, and hematoma in one image. XRES imaging depicted 17 normal findings and 33 abnormalities. In one image, XRES imaging clearly depicted a cyst where compound imaging remained questionable (Fig. 3).

TABLE 1. Median Scores and Statistical Analysis for Abdominal Imaging

Evaluation Criteria	Compound Imaging (SonoCT imaging only)	Compound with XRES Imaging Applied	*P*
Borders	4 (3–5)	5 (4–6)	0.001
Contrast	5 (4–6)	5 (4–6)	0.001
Noise	4 (3–6)	5 (5–6)	0.001
Quality	4 (4–5)	5 (5–6)	0.001

Data are median scores (range) based on a six-point rating scale. P is based on the results of the Wilcoxon signed rank pairwise test for differences between conventional and XRES imaging.

TABLE 2. Median Scores and Statistical Analysis for Small Parts Imaging

Evaluation Criteria	Compound Imaging (SonoCT imaging only)	Compound with XRES Imaging Applied	*P*
Borders	5 (4–6)	6 (5–6)	0.001
Contrast	5 (4–6)	6 (5–6)	0.001
Noise	5 (4–6)	6 (5–6)	0.001
Quality	5 (4–6)	6 (5–6)	0.001

Data are median scores (range) based on a six-point rating scale. P is based on the results of the Wilcoxon signed rank pairwise test for differences between conventional and XRES imaging.

Pediatric Imaging

The median scores of the compound and XRES pediatric examinations for all criteria are shown in Table 3. Regarding abnormality detection, compound and XRES imaging depicted the same 43 normal findings and 7 abnormalities. Abnormalities included ovarian torsion in 3 images, appendicitis in 2 images, and hydronephrosis in 2 images.

Statistical Analysis

Compared with the US examination using compound imaging only, XRES imaging of abdomen, small parts and pediatrics scored higher for all evaluated judgment criteria and applications (Tables 1-3). Differences in borders delineation ($P < 0.05$), tissue contrast ($P < 0.05$), amount of noise ($P < 0.05$), and overall quality ($P < 0.05$) reached statistical significance.

According to the Kruskal–Wallis one-way analysis of variance by ranks, the comparisons of median scores for each judgment criteria showed inhomogeneous improvements. Improvement in tissue contrast was significantly higher for small parts and pediatric imaging than for abdominal imaging ($P < 0.05$). Improvement in border delineation and in quality, as well as reduction of the amount of noise, were not statistically different among the 3 US application types (abdominal, small parts, pediatric).

DISCUSSION

New technologies in medical US imaging are regularly introduced to improve image quality and diagnostic conspicuity. Real-time processing involving adaptive image analysis and enhancement (XRES imaging), a by-product of image processing originally developed for MRI, is one of the latest

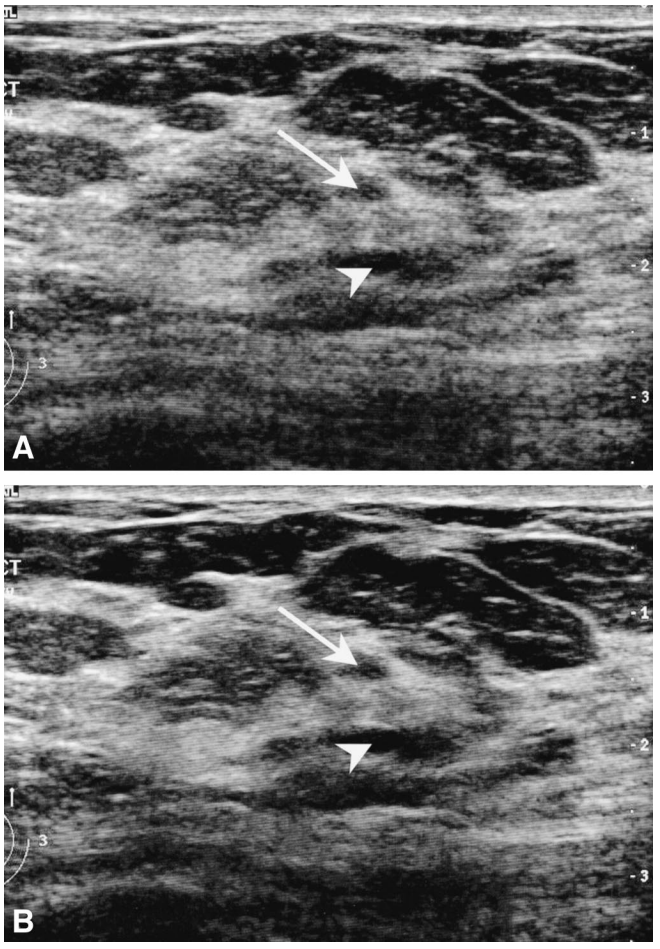

FIGURE 3. Longitudinal view of the external upper quadrant of the right breast. A, Compound image. Two dark spots are visible in the middle of the picture (arrow and arrowhead). No definite diagnosis of cyst (sharp margin, anechogenicity) could be made. B, XRES image. The superficial spot (arrow) proves to be a fatty lobule. The lower spot (arrowhead) becomes anechogenic and well demarcated, what increases the likehood of cyst. The cystic nature of the lesion was subsequently proven by fine needle aspiration.

developments. Various adaptive algorithms have been described previously in the literature,[11,12] but none achieved commercial development. Furthermore, to our knowledge, the effect of the postprocessing was never assessed in a clinical study.

Our study findings demonstrated that this real-time technology enhanced definition of anatomic structures and borders, enhanced tissue contrast, reduced noise, and improved overall image quality. These improvements were identified for low-frequency imaging (abdominal US) as for high-frequency imaging (small parts and pediatric US). Improvements were not identical for all applications; thus, contrast enhancement was significantly lower for low-frequency imaging than for high-frequency imaging. One XRES-processed image revealed a pathologic condition that was questionable before the processing. This was a breast cyst of 3 millimeters in size.

TABLE 3. Median Scores and Statistical Analysis for Pediatric Imaging

Evaluation Criteria	Compound Imaging (SonoCT imaging only)	Compound with XRES Imaging Applied	*P*
Borders	5 (4–5)	6 (5–6)	0.001
Contrast	5 (4–6)	6 (5–6)	0.001
Noise	5 (4–6)	5.5 (5–6)	0.001
Quality	5 (4–6)	6 (5–6)	0.001

Data are median scores (range) based on a six-point rating scale. *P* is based on the results of the Wilcoxon signed rank pairwise test for differences between conventional and XRES imaging.

Generally speaking, adaptive algorithms modify the image on the basis of a computerized analysis on the pixel level. They recognize structures, orientation and intensity of image points, and enhance, reduce or even delete the pixel, following the programmed algorithm.[10–15] At the most, this processing may totally make clinically useful information vanish. Our study demonstrated that all abnormalities seen with SonoCT imaging were also visible after applying XRES imaging. In addition, no degradation was encountered, whatever the regarded application or parameter.

US is basically a dynamic diagnostic procedure. Not only are the patterns of anatomic structures taken in account for diagnosis, but also their movements, stiffness under the probe, and appearances from multiple angles of view are noted. The diagnosis is assumed during the dynamic examination. Freeze frames are only taken for documentation purposes. Thus, in our study, the dynamic parameters were obscured. We compared still images chosen by sonographers for their informative contents. If there were abnormalities, the pathologic process would be depicted clearly on the conventional image, with the best angle of view. With such a methodology, depiction of a new pathologic process in the XRES-processed image could only be regarded as incidental. To compare accurately the diagnostic efficiency of the 2 techniques, a twin real-time examination would have been necessary: one with SonoCT imaging only, the other one with SonoCT and XRES modes. Comparative evaluation of images would be lost with such a method, as the scanning plane would have been necessarily different. Furthermore, 2 different sonographers would have performed examinations, each being blinded from the findings of the other. Thus, the sonographers would be evaluated with such a method, and not technology.

We observed that the algorithm used by XRES processing had no homogeneous repercussions on the evaluated applications and parameters. Contrast improvement, although present for all applications, was significantly weaker for low-frequency examinations than for high-frequency examinations. This result could be an effect of the chosen parameters of the adaptive algorithm; this brings up the question of the specificity of the algorithms for the different applications. The body habitus of adult patients could also have an influence on the suboptimal contrast results for low-frequency applications. As the parameter of body constitution was not evaluated in our study, its impact on adaptive processing remains questionable. Furthermore, as only one solid focal liver lesion was included in the analyzed images, we may rule on contrast between normal anatomic structure but not forecast the effects of the processing in the context of solid visceral lesions.

Another way to understand the inhomogeneity of the effect on tissue contrast would be to consider difficulties for the readers to identify clearly contrast on the images. There were fundamental differences between the sonographically explored structures: they were fine and detailed for high-frequency examinations and more coarse and wide for low-frequency examinations. We know from plain radiography analysis that low-contrast differences are difficult to observe on large surfaces, whereas they are easier to assess on fine structures. The observed differences could be related to this phenomenon.

The evaluation of the images directly on the standard monitor of the ultrasound machine would have been the optimal way to proceed. Unfortunately, random screening of paired images was not possible on such a monitor. Thus, the images were processed between acquisition in the US machine and matched display for evaluation. From their original DICOM format, the pictures were saved as JPEG images, using a low compression ratio. We know from previous studies that this processing is acceptable, with minimal loss of information.[16–18] All of our images had undergone the same processing. So, if any distortion was introduced by compression, it remained the same for the entire series and did not influence evaluation.

In conclusion, real-time adaptive image processing, as implemented on our US machine, enhances border definition, enhances tissue contrast, reduces noise, and enhances overall image quality, without degradation of diagnostic informative contents of images. The impact of this processing on diagnostic efficiency was not evaluated. Further studies, with targeted methodology, have to be performed to resolve this question.

ACKNOWLEDGMENTS

We thank Nicole Dagon, Ilse Tellez, Margrit Moser, Pierre Frossard, Jüdith Künzli, Catherine Le Saux, Pascal Ledermann, Line Demarta and Françcois Guignard, sonographers of the Department of Diagnostic and Interventional Radiology, for their kind assistance for image acquisition. We also thank Sherif Makram-Ebeid and Jacques Souquet of Philips Research, along with Cedric Chenal and James Jago of Philips Ultrasound for their assistance with the description of XRES processing.

REFERENCES

1. Hann LE, Bach AM, Cramer LD, et al. Hepatic sonography: comparison of tissue harmonic and standard sonography techniques. *AJR Am J Roentgenol*. 1999;173(1):201–206.
2. Shapiro RS, Wagreich J, Parsons RB, et al. Tissue harmonic imaging sonography: evaluation of image quality compared to conventional sonography. *AJR Am J Roentgenol*. 1998;171(5):1203–1206.
3. Blaivas M, DeBehnke D, Sierzenski PR, et al. Tissue harmonic imaging improves organ visualization in trauma ultrasound when compared with standard ultrasound mode. *Acad Emerg Med*. 2002;9(1):48–53.
4. Saleh A, Ernst S, Grust A, et al. [Real-time compound imaging: improved visibility of puncture needles and localization wires as compared to single-line ultrasonography]. *Rofo Fortschr Geb Rontgenstr Neuen Bildgeb Verfahr*. 2001;173(4):368–372.
5. Entrekin RR, Porter BA, Sillesen HH, et al. Real-time spatial compound imaging: application to breast, vascular, and musculoskeletal ultrasound. *Semin Ultrasound CT MR*. 2001;22(1):50–64.
6. Jespersen SK, Wilhjelm JE, Sillesen H. In vitro spatial compound scanning for improved visualization of atherosclerosis. *Ultrasound Med Biol*. 2000;26(8):1357–1362.
7. Rosen EL, Soo MS. Tissue harmonic imaging sonography of breast lesions: improved margin analysis, conspicuity, and image quality compared to conventional ultrasound. *Clin Imaging*. 2001;25(6):379–384.
8. Huber S, Wagner M, Medl M, et al. Real-time spatial compound imaging in breast ultrasound. *Ultrasound Med Biol*. 2002;28(2):155–163.
9. Burt P, Adelson E. The Laplacian pyramid as a compact image code. *IEEE Trans Com*. 1983;COM-31:532–540.
10. Weickert J. Foundations and applications of nonlinear anisotropic diffusion filtering. *Zeitschrift für angewandte Mathematik und Mechanik*. 1996;76(Supp 1):283–286.
11. Bamber JC, Phelps JV. A real-time implementation of coherent speckle suppression in B-scan images. *Ultrasonics*. 1991;29(3):218–224.
12. Loupas T, McDicken N, Anderson T, et al. Development of an advanced digital image processor for real-time speckle suppression in routine ultrasound scanning. *Ultrasound Med Biol*. 1994;20(3):239–249.
13. Weickert J, ter Haar Romery B, Viergever M. Efficient and reliable schemes for nonlinear diffusion filtering. *IEEE Trans Image Processing*. 1998;7(3):398–410.
14. Bamber JC, Daft C. Adaptive filtering for reduction of speckle in ultrasonic pulse-echo images. *Ultrasonics*. 1986;24(1):41–44.
15. Stetson P, Sommer F, Macovski A. Lesion contrast enhancement in medical ultrasound imaging. *IEEE Trans Med Imaging*. 1997;16(4):416–425.
16. Li F, Sone S, Takashima S, et al. Effects of JPEG and wavelet compression of spiral low-dose CT images on detection of small lung cancers. *Acta Radiol*. 2001;42(2):156–60.
17. Persons KR, Palisson PM, Manduca A, et al. Ultrasound grayscale image compression with JPEG and wavelet techniques. *J Digit Imaging*. 2000;13(1):25–32.
18. Karson TH, Chandra S, Morehead AJ, et al. JPEG compression of digital echocardiographic images: impact on image quality. *J Am Soc Echocardiogr*. 1995;8(3):306–318.